Chapter 6

Mechanical Behavior of Zr-Based Metallic Glasses and Their Nanocomposites

Devinder Singh, R.K. Mandal, R.S. Tiwari and O.N. Srivastava

Additional information is available at the end of the chapter

http://dx.doi.org/10.5772/64221

Abstract

In the present chapter, results of our recent investigations on the role of gallium (Ga) on the aluminum (Al) site in $Zr_{69.5}Al_{7.5-x}Ga_xCu_{12}Ni_{11}$ metallic glass (MG) composition have been discussed. The material tailoring and cooling rate effects on the mechanical behavior of Zr-based metallic glasses and their nanocomposites have been studied. The substitution of Ga on the Al site in Zr–Al–Cu–Ni alloy affects the nucleation and growth characteristics of quasicrystals (QCs) and consequently changes the morphology of nanoquasicrystals. The $Zr_{69.5}Al_{7.5-x}Ga_xCu_{12}Ni_{11}$ system displayed metallic glass formation in the range of x = 0–7.5. In this process, we have come out with a new glass composition; Zr-Ga-Cu-Ni with glass transition temperature (T_g)—614 K. The effect of cooling rate on the glass forming ability (GFA) and mechanical properties for this new metallic glass composition has been discussed and compared with some other Zr-based metallic glasses. The various indentation parameters such as microhardness, yield strength, strain hardening constant, nature of shear band formation, and so on for the alloys have been analyzed. The study is focused on investigations of these materials to understand the structure (microstructure) property correlations.

Keywords: metallic glasses, quasicrystal, composites, mechanical properties, cooling rate

1. Introduction

Metallic materials are traditionally considered as crystalline in nature, possessing translational as well as orientation symmetry, i.e., their constituent atoms are arranged in a regular and periodic manner in three dimensions. However, a revolution in the concept of metals was

brought, when metallic glasses (MGs) and quasicrystals (QCs) have been discovered. MGs are amorphous in nature possessing short-range ordering while QCs possess aperiodic long-range order associated with crystallographically forbidden rotational symmetries. Both quasicrystal-forming alloys and MGs giving rise to nanoquasicrystalline phase on annealing have attracted attention owing to their promise to qualify for many potential applications.

1.1. Metallic glasses

Ever since the formation of first metallic glass in the Au–Si system by rapid solidification, numerous investigations have been carried out over the past 15 years due to their attractive properties and technological potential. In initial period of metallic glass study, high cooling rates of the order of 10^5 to 10^6 K/s were the usual requirement for the formation of glassy phase. However, in the recent years, a new class of metallic glass known as bulk metallic glass (BMG) has been synthesized using very slow cooling rates. These newly developed BMGs have generated immense research activity driven by both a fundamental interest in the structure and properties of disordered materials and their unique promise for structural and functional applications. MGs have very high-yield strength and very high elastic limit compared to crystalline steel and Ti alloys (**Figure 1(a)**). They have very high fracture strength coupled with 2–3% of elastic strain. Conventional aluminum, titanium alloys and steels can sustain 1–2% of elastic strain. The glasses have tensile yield strength ($\sigma \sim$ 1.9 GPa), i.e., a high strength-to-weight ratio, making them a possible replacement for Al, but with a much greater resistance to permanent, plastic deformation (i.e., fracture toughness). A large domain of high fracture strength and elastic strain can be achieved by nanocrystallization into the amorphous matrix. **Figure 1(b)** represents the highest strength, specific strength and specific Young's modulus of any bulk amorphous or crystalline metal.

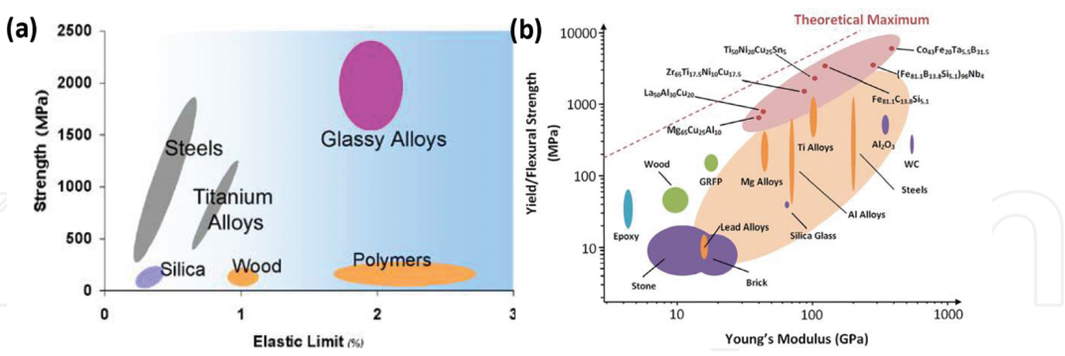

Figure 1. (a) Amorphous metallic alloys combine higher strength than crystalline metal alloys with the elasticity of polymers [1]. (b) Schematic representation of room temperature yield (metals, composites, and polymers) or flexural strength (ceramics) as a function of modulus. Note the increased strength of amorphous metals over conventional crystalline metals [2].

MGs possess a number of very attractive properties, and in many cases, these properties are enhanced by suitable heat treatment. The ability to store a high amount of elastic energy has made this material to use as a potential spring material. This has led to its first and most visible use in the heads of golf clubs. The addition of ceramic second-phase particles into the material

improves its ductility. This composite can be used in aircraft frames and automobiles as armor penetrator material and medical implants. Due to large super-cooled liquid regions, the workability of these materials is very high. This property has been applied in friction welding of Pd-based bulk MGs [3]. The high strength, hardness, fracture toughness, and fatigue strength of MGs make them ideal for the use as optical, die, tool, and cutting materials [4, 5].

Among the large number of multicomponent glassy alloy systems, Zr-based MGs have outstanding glass forming ability (GFA). The exceptionally high-yield strength, close to the theoretical limit, high hardness, and elastic modulus of these MGs offer them potential for structural applications. However, plastic deformation at room temperature occurs in a highly localized manner by the formation of shear bands. In these MGs, the definitive correlations between mechanical behavior and atomic structures have not been clearly understood.

1.2. Quasicrystals

Another important class of material is QCs. The breakthrough experiments by Shechtman et al. on rapidly solidified Al-14% Mn alloys have created a new concept of nonperiodic atomic arrangements with only orientational order, which exhibit sharp diffraction peaks with five-fold symmetry [6]. This new form of ordered structures having orientational order and lacking strict translational periodicity was designated as "quasicrystal" by Levine and Steinhardt [7]. It may be noted that in contrast to both crystal and QCs, amorphous solids possess neither orientational nor translational order. Most familiar quasicrystalline systems are Al-, Ti-, and Mg-based binary and ternary alloys, though there have been a few reports in other systems such as Cd-Mg-Yb, Ag-In(Cd), Al-Zn-Ce, and Cu-Ga-Mg-Sc, etc. The discovery of the quasicrystalline phases has also generated a great deal of interest in regard to complex crystalline structures known as approximant phases, which have remarkable similarities with their parent quasicrystalline structures. These often coexist with QCs and have similar chemical compositions and similar electron diffraction patterns (**Figure 2**). Quasicrystal approximants have similar local atomic structures to QCs [8–12]. Because of these structural similarities, the search for other possible phases as well as intensive investigations of their phase transformation has

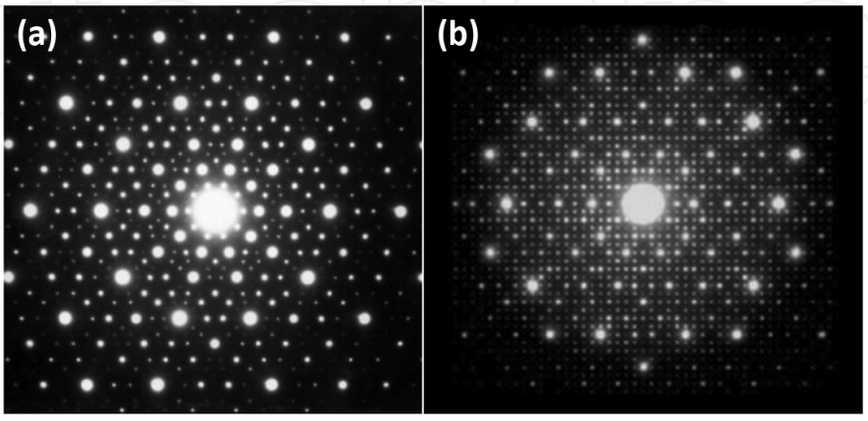

Figure 2. Selected area diffraction patterns of (a) icosahedral quasicrystal showing five-fold symmetry in Al-Mn and (b) pseudodecagonal quasicrystal approximant in Al-Co-Ni alloy [6, 12].

become quite pertinent in connection with the determination of the phase stability of quasicrystalline system.

The successful applications of QCs are very limited. QCs are corrosion resistant and have low coefficients of friction, and thus, they can be used as a surface coating for frying pans. They can also be used in wear resistant coatings. Al-based quasicrystalline alloys, e.g., Al-Mn-Ce containing nanoicosahedral particles may be used in surgical blades. Ti- and Zr-based QCs could be incorporated into hydrogen storage materials.

1.3. Nanocomposites

Quasicrystal forming alloys and MGs promise to qualify for many potential applications. However, bulk QCs are mostly brittle and this problem can be surmounted by producing glass-nanocrystal (nc)/nanoquasicrystal (nqc) composites ($Zr_{69.5}Al_{7.5}Cu_{12}Ni_{11}$) through controlled crystallization of MGs. Quasicrystal evolution from metallic glass systems may provide a way to produce nanostructured quasicrystalline alloys with attractive mechanical properties. The advantage of formation of quasicrystalline phase through devitrification of MGs is also due to the fact that the microstructure can be precisely controlled. The control of microstructure is very important as the optimum property design is related to the microstructure. It has been pointed out that Ti- and Zr-rich alloys have significantly higher hardness in the nanoquasicrystalline state (755 and 610 VHN, respectively) compared to the amorphous state in melt-spun condition. The hardness values of Ti- and Zr-rich alloys increase further by nanoquasicrystallization of the amorphous phase to 810 and 620 VHN, respectively. Misra et al. [13] have studied the plastic deformation in nanostructured bulk glass composites during nanoindentation. The structural changes are accompanied by decrease in specific volume, bulk modulus and Poisson's ratio. Small specific changes upon primary devitrification suggest a close relationship between the glassy structure and the icosahedral structure.

2. Effect of material tailoring on the mechanical properties

Elemental substitution is widely used to find new MGs and QCs with improved properties. In this section, the role of Ga on the Al site in $Zr_{69.5}Al_{7.5-x}Ga_xCu_{12}Ni_{11}$ metallic glass composition has been discussed. The alloy design principle adopted in arriving at Ga-substituted glass compositions pertains to retaining the valence electron ratio (e/a) constant. In this respect, Ga substitution on the Al site seems to be ideal. The substitution of Ga in $Zr_{69.5}Al_{7.5-x}Ga_xCu_{12}Ni_{11}$ alloys results in a change from a two-step crystallization ($x = 0$) to a single-step one ($x = 7.5$) [14, 15]. For $x = 0$, we have the well investigated Zr-based alloy; and for $x = 7.5$, we have come out with a new composition of glass with $T_g = 614$ K [16–20]. The effect of the said material tailoring on the mechanical properties of these alloys has also been studied. The recent emphasis on nanostructured materials and synthesis of MGs has added a new dimension to the study of their indentation behavior. Indentation studies offer opportunities to investigate the fundamental nature of deformation in glasses and their composites from a relatively small volume

of material. The indentation size effect (ISE) and shear band formation under compression are able to throw light on the mechanical behavior of materials.

2.1. Microstructural and structural features

The $Zr_{69.5}Al_{7.5-x}Ga_xCu_{12}Ni_{11}$ (x = 0, 1.5, and 7.5) MGs with a thickness of ~40–50 μm and lengths of ~1–2 m have been synthesized using melt spinning technique [19, 21]. **Figure 3(a)** shows the macroscopic image of the melt-spun ribbons synthesized at 40 m/s. **Figure 3(b)** and the inset therein show the transmission electron microscopy (TEM) image and corresponding selected area diffraction pattern (SADP) displaying diffuse halos for $Zr_{69.5}Al_{7.5-x}Ga_xCu_{12}Ni_{11}$($x$ = 7.5) alloy. We note that the TEM bright-field micrograph displayed no discernible contrast. This clearly indicates the formation of glassy phase in the system and similar features were observed for x = 0 and 1.5. The glass-nc/nqc composites are produced after controlled crystallization of melt-spun ribbons corresponding to compositions x = 0, 1.5, and 7.5 [19–21]. The TEM micrograph of these composites is shown in **Figure 4**. Inset in them demonstrates the presence of crystalline/quasicrystalline particles embedded in the glassy matrix. The composition of the alloys with $x > 1.5$ consists of icosahedral and Zr_2Cu phases embedded in the glassy matrix. The finer grains of both these phases have been observed in the Ga-bearing glass composition (x = 7.5) [19]. The grain refinement of quasicrystals with respect to Ga substitution may be understood by recalling expression [22, 23] of the steady-state nucleation rate (I^s) and is reproduced below

$$I^s = A\exp[(-16\Pi\sigma^3)/(3KT(\Delta G_v)^2)] \quad (1)$$

where 'A' is known as dynamical prefactor and is a function of the atomic mobility at the nuclei-liquid/glass interface. ΔG_v = driving free energy per unit volume for the phase transformation. According to classical theory of nucleation, the nucleation barrier is controlled by interfacial free energy (σ) between the nuclei and the liquid/glass [22]. The decrease in σ between the icosahedral quasicrystalline nuclei and the liquid with increasing Ga content leads to the

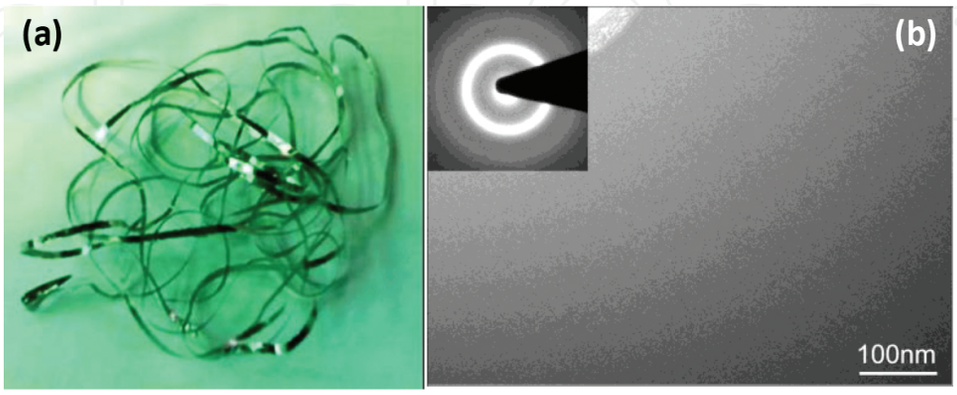

Figure 3. (a) Optical image showing the formation of long melt-spun ribbons synthesized at 40 m/s. (b) TEM image and the corresponding diffraction pattern of as-synthesized $Zr_{69.5}Ga_{7.5}Cu_{12}Ni_{11}$ alloy. (Reprinted with kind permission from references [15, 19], Copyright 2015 and 2011, Elsevier.)

increase in the nucleation rate. The reported interfacial energy per unit area of Ga (~0.6 J/m^2) is less than that of Al (~1.2 J/m^2) [24–26]. Thus, it can be said that the substitution of Ga reduces the interfacial energy between quasicrystal and remaining amorphous phase, thereby increasing the nucleation rate of the crystalline/quasicrystalline phases. The formation of icosahedral phase has been observed for all the annealed glasses. Thus, the icosahedral order presents predominantly in the supercooled liquid for all the samples (x = 0–7.5).

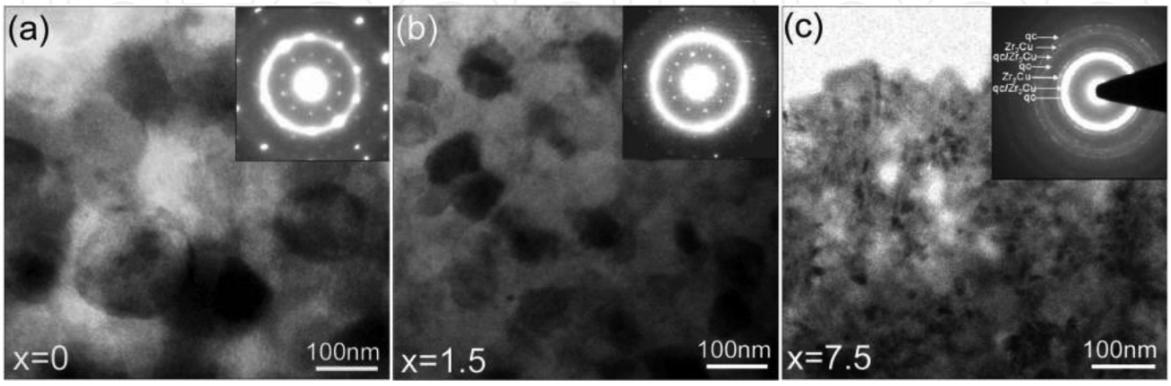

Figure 4. TEM microstructures and the corresponding diffraction patterns of $Zr_{69.5}Al_{7.5-x}Ga_xCu_{12}Ni_{11}$ alloy with x = 0 (a), x = 1.5 (b), and x = 7.5 (c) formed after heat treatment. (Reprinted with kind permission from reference [19], Copyright 2011, Elsevier.)

The composition of the alloys (in at.%) based on electron probe microanalysis (EPMA) has been found to be $Zr_{69.6}Al_{7.6}Cu_{12.5}Ni_{10.3}$ (for x = 0), $Zr_{69.2}Al_{6.2}Ga_{1.6}Cu_{12.8}Ni_{10.2}$ (for x = 1.5), and $Zr_{69.4}Ga_{7.7}Cu_{12.5}Ni_{10.4}$ (for x = 7.5). The presence of oxygen within the detectable limit of EPMA was not found.

2.2. Mechanical properties

In this section, we present the results of micro-/nanoindentation behavior of the three glassy compositions and their respective composites. **Figure 5** depicts the images of microindent for the as-synthesized and annealed ribbons of x = 7.5. It has been observed that a number of shear

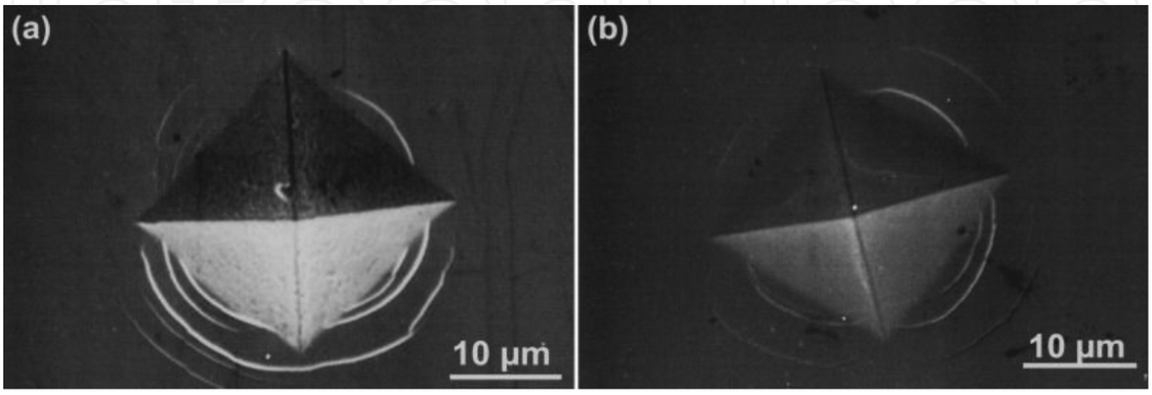

Figure 5. SEM micrographs for the as-synthesized (a) and annealed ribbons (b) of x = 7.5 displaying shear bands. (Reprinted with kind permission from reference [19], Copyright 2011, Elsevier.)

bands decrease gradually in the annealed condition as compared to that of glassy state. At this stage, the indentation behavior is governed by the volume fraction of nanocrystalline/nanoquasicrystalline phases. Thus, the glass-nc/nqc composite possesses different indentation characteristics as is seen in the case of x=7.5 that Zr_2Cu intermetallic phase exists along with the nqc phase, which inhibits the propagation of shear bands in the glassy matrix during indentation. We note from **Table 1** that annealed ribbons for x = 7.5 display the highest microhardness value (~10 GPa). The microhardness values for x = 1.5 at 300 g load are ~4.81 and ~5.89 GPa for as-synthesized and annealed samples, respectively. These are quite close to that of Zr-Al-Ni-Cu-Ag and Zr-Al-Ni-Cu-Nb MGs and their nqc composites [27].

x	As-synthesized ribbons			Annealed ribbons		
(at.%)	Microhardness (GPa) at 100 g load (±0.1)	Nanohardness (GPa) at 5000 μN (±0.2)	Reduced Modulus (GPa) at 5000 μN (±5.0)	Microhardness (GPa) at 100 g load (±0.1)	Nanohardness (GPa) at 8000 μN (±0.2)	Reduced Modulus (GPa) at 8000 μN (±5.0)
0	4.7	8.7	98	6.7	11.5	115
1.5	6.1	9.5	112	7.5	12.8	136
7.5	6.6	11.8	140	10.1	14.4	151

Table 1. Mechanical properties of as-synthesized and annealed ribbons of $Zr_{69.5}Al_{7.5-x}Ga_xCu_{12}Ni_{11}$ (x = 0, 1.5, and 7.5) alloys. (Reprinted with kind permission from reference [19], Copyright 2011, Elsevier).

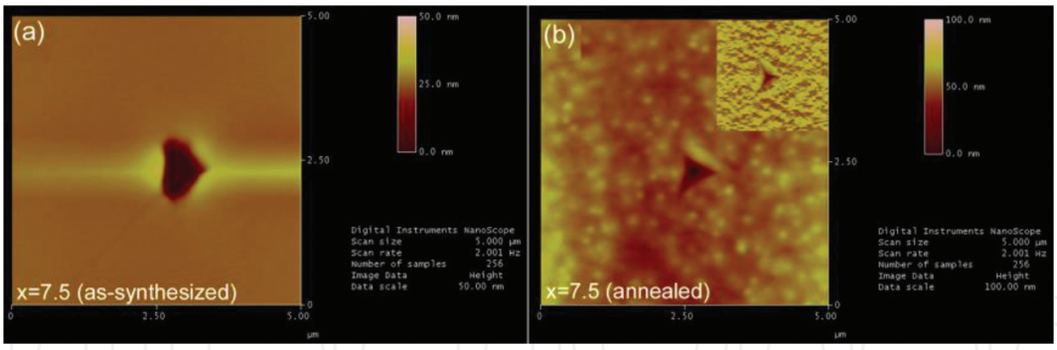

Figure 6. AFM observation of the nanoindentation imprints from the as-synthesized (a) and annealed ribbon (b) of x = 7.5 at 5000 μN. The inset of (b) showing the tip image of nanoindenter [19].

To study the nature of indentation at submicroscopic scale as well as the plastic deformation of composites containing nc/nqc phases, we now present the results of nanoindentation. The indentation impressions of Berkovich indenter at 5000 μN for x = 7.5 are shown in **Figures 6(a)** and **(b)**. These are to compare the indentation impressions of the glassy phase with that of their nanocomposite. The inset in **Figure 6(b)** shows the tip image of the nanoindenter. We note clearly the presence of fine grains in **Figure 6(b)** that are absent in **Figure 6(a)**. The size of the indentation impression changes with partial crystallization and no cracking occurred. The height contrast around the indents is due to pileup. The contrast of the pileup

in glassy sample is much more prominent as compared to that of annealed ribbons. The formation of pileups around the indents must be related to shear banding operations and are extensively observed in amorphous alloys [28–32].

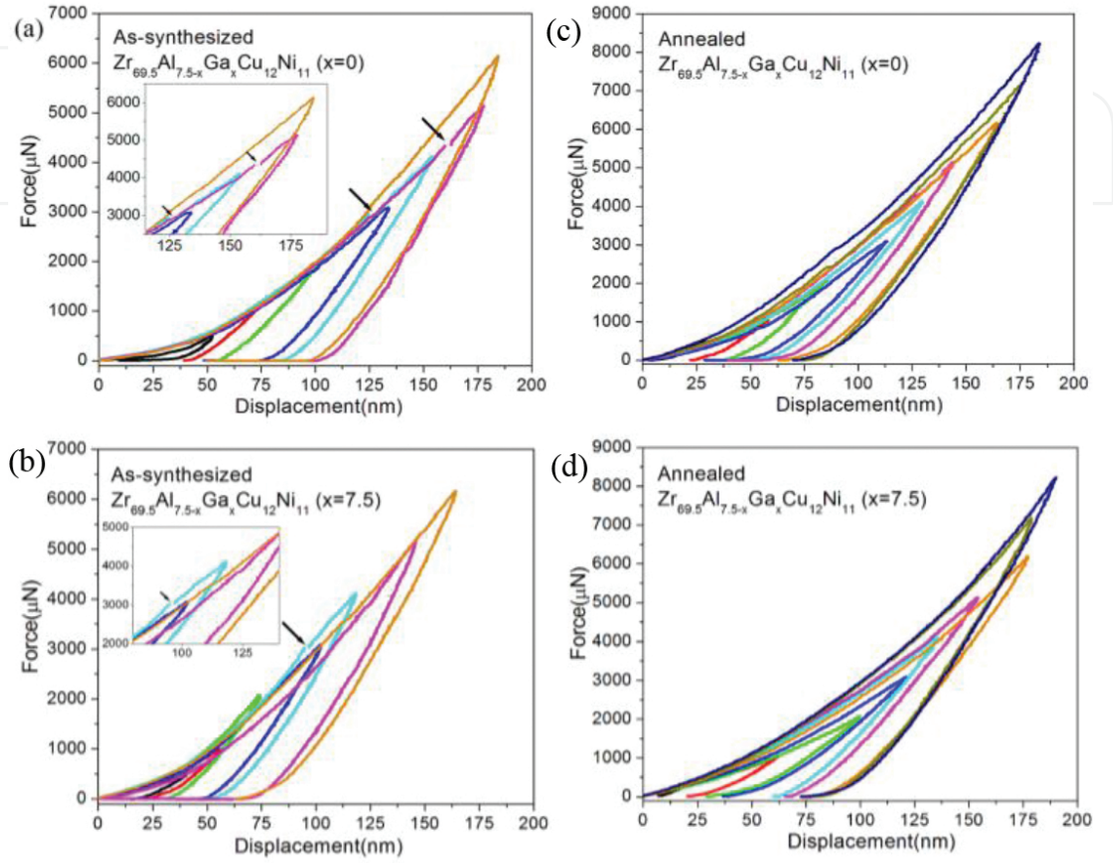

Figure 7. Plot of the indentation force (*P*) versus indenter displacement (*h*) obtained from nanoindentation tests for the as-synthesized (a and b) and annealed (c and d) ribbons of $x = 0$ and 7.5 respectively [19].

Figures 7(a) and **(b)** depict the load (*P*) versus depth (*h*) behavior of melt-spun ribbons, whereas **Figures 7(c)** and **(d)** display the *P* versus *h* characteristics of their respective composites. The values of nanohardness and reduced modulus for $x = 0$, 1.5, and 7.5 are given in **Table 1**. The values of nanohardness for the glassy alloys ($x = 0$–7.5) are in the range of ~9–12 GPa. Reduced modulus is sensitive to compositions of the alloy as well as atomic arrangements. The reduced modulii for the glassy alloys ($x = 0$–7.5) lies in the range of ~98–140 GPa. These values of nanohardness and reduced modulus are comparable to those of the Zr-based alloys [33–35]. It can be seen from **Table 1** that composites have higher micro- /nanohardness values than those of glassy alloys. Ramamurty et al. [36] reported that the presence of nanocrystalline particles in the glassy matrix significantly improves the stiffness and strength values. The nanohardness value (mean contact pressure) is higher than that of Vickers hardness value [37]. The difference in the values is primarily due to two reasons: (i) indentation size effect and (ii) actual and projected area of contacts, respectively, for nano- and microhardness measurements.

http://dx.doi.org/10.5772/64221

We have observed pop-ins during loading (marked by the arrow in **Figures 7(a)** and **(b))** for the melt-spun ribbons. These pop-ins indicate displacement bursts that signify the formation of shear bands [38]. The pop-ins are prominent in amorphous alloys while the presence of these is either less prominent or even completely suppressed in case of annealed alloys. Our observation is in agreement with the results reported by others [29, 38, 39]. The pop-ins are absent in composites and this may be attributed to the presence of nc/nqc grains in the glassy matrix. The nature of deformation can be influenced by structural features while the chemistry affects such behavior in a quantitative way. This is the reason why we observe similar kind of P versus h curves corresponding to x = 0 and 7.5 after crystallization of the glasses. The observation of pop-ins during loading cannot be attributed to the process of nanocrystallization as noted in reference [40]. The break in the P versus h curves for such a case should appear while unloading. To settle this issue experimentally, the TEM investigations of the indented portion of these samples have been done. The bright-field images of the thinned specimens for the glassy alloys with x = 0 and 7.5 are shown in **Figures 8(a)** and **(b)**. The preparation of these samples was done by masking the indented side and thinning was done from the opposite side. The bright-field images resemble analogous to those shown in **Figure 3(b)** and do not show any regions of residual contrast. The curvilinear line (marked by arrows) has given evidence of layer wise displacement separated by boundary. These lines must be related to the shear banding operations, and thus, the possibility of nanocrystallization has been ruled out.

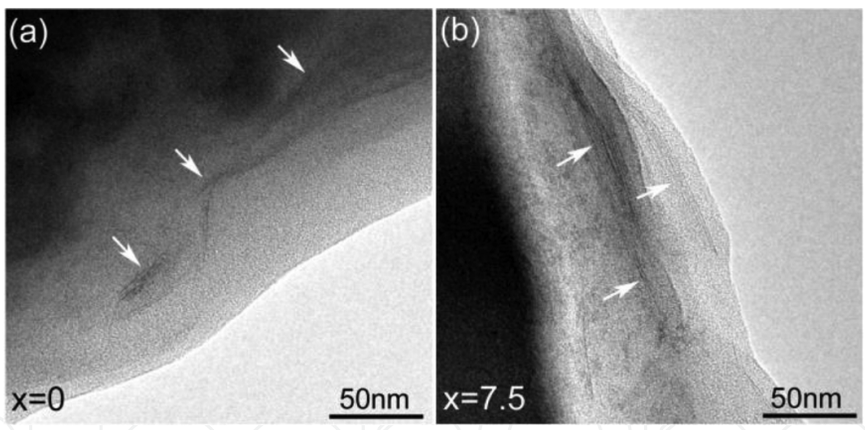

Figure 8. Bright-field TEM images of the indented portion of as-synthesized thinned specimens for x = 0 and 7.5. (Reprinted with kind permission from reference [19], Copyright 2011, Elsevier.)

The change in the mechanical behavior of MGs and their composites can be understood on the basis of free volume model. In the present case, the variation of free volume with Ga substitution may increase the hardness of the MGs. The atomic radius of Ga (0.141 nm) is intermediate between the atomic radius of Al (0.143 nm) and Ni (0.125 nm) and the atomic radius of Zr (0.160 nm) and Cu (0.128 nm). Thus, the substitution of Ga may increase the packing density of the alloy and this would lead to the decrease in the free volume [41]. The high resistance to plastic deformation under applied stress may be attributed to a low free volume [42]. The increase in the hardness of MGs with alloying addition has been reported recently [41]. The shear transformation zones (STZs) are the primary carriers of plasticity in amorphous

materials [43, 44]. The formation of STZs depends upon the availability of free volume. The precipitation of nc/nqc phases in the case of composites decreases the free volume and this causes densification of the metallic glass [45]. This results in an increased resistance to plastic deformation and therefore enhancement of hardness of the metallic glass upon structural relaxation and nanocrystallization. This observation is consistent with the results reported earlier [46, 47]. In the case of glass-nc/nqc composites, the hardness increases with increase in Ga addition. This may be due to the grain refinement of nanocrystals/nanoquasicrystals that produces many interfaces leading to the strengthening phenomenon.

3. Effect of cooling rate on the mechanical properties

The absence of grain boundaries and dislocations in MGs contributes to its exceptional properties [48–53]. MGs lack long-range order and thus, they can be considered as solids with frozen-liquid structures composed of tightly bonded atomic clusters and free volume zones [54–56]. The frozen-in excess volume is often interpreted as an increase of free volume content in the MGs [57, 58]. The functional and mechanical properties of a metallic glass are determined by its internal atomic configuration [59, 60]. The different variables such as the cooling rate and composition affect the structure of MGs [14, 61, 62]. Among these, the critical cooling rate is a very important factor that plays a crucial role in determining the atomic structure and hence deformation behavior of MGs [63–65]. The limited macroscopic plastic strain before fracture of MGs constrains their applications [43]. Plastic deformation of MGs is localized within relatively thin regions called shear bands, resulting in a very low macroscopic plastic flow limit [13, 43, 66]. Recent investigations show that the plastic strain of some monolithic MGs can be improved by enhancing the homogeneity in microstructure through the high cooling rate [67]. The high cooling rate may result in the configurationally looser atomic packing and thus more free volume zones, which therefore contribute to larger plasticity. Chen et al. [68] suggested that the plasticity for MGs can be tailored by applying different cooling rates during solidification. Jiang et al. [69] found that the Cu-based bulk metallic glass (BMG) is having higher hardness as compared to its ribbon counterpart of the same composition but synthesized at a much higher cooling rate. It has been observed that decreasing the cooling rate of glass forming promoted the formation of denser atomic configuration in the resultant alloy [57]. The study of cooling rate effect on the nanomechanical response for a Ti-based BMG reveals that the hardness increases while the plastic deformation gradually decreases from the edge to the center of the sample [70]. Recently, Huang et al. [71] reported the effect of cooling rate on the local atomic ordering and the wear behavior of Zr-Cu-Al-Ag BMG. These results indicate that the cooling rate used during glass formation is a processing parameter that may be tuned to change the mechanical properties of MGs.

The effect of cooling rate on the mechanical behavior of $Zr_{69.5}Ga_{7.5}Cu_{12}Ni_{11}$ metallic glass has been studied using microindentation technique. The ribbons of alloy have been synthesized at three cooling rates, corresponding to wheel speeds of 30, 40, and 50 m/s. The different properties such as glass forming indicators, structural relaxation heat, microhardness, yield strength, strain-hardening constant, material constant related to the resistance of the metal to

penetration and pileup parameter pertaining to nature of shear band are expected to throw light on the internal structure of glass. They are compared and discussed with respect to the rate of cooling. This study provides some insights to understand the correlation between the cooling rate and the mechanical behavior of Zr-Ga-Cu-Ni metallic glass.

3.1. Microstructural and structural features

Figure 9 shows the X-ray diffraction (XRD) patterns of as-synthesized $Zr_{69.5}Ga_{7.5}Cu_{12}Ni_{11}$ melt-spun ribbons synthesized at different wheel speeds. It has been observed that all the patterns of the alloys consist of only broad diffraction maxima (at the position $2\theta \approx 36°$) without a detectable sharp Bragg peak. This shows formation of a glassy phase. The XRD pattern of the ribbon synthesized at 40 m/s revealing the presence of a glassy phase exhibits greater peak broadening and lower XRD intensity as compared to the ribbons synthesized at 30 m/s. These effects are more pronounced by further increasing the wheel speed to 50 m/s. The full width at half maximum (FWHM) was found to be 5.5°, 4.7°, and 3.9° for the ribbons synthesized at 50, 40, and 30 m/s, respectively. These results indicate that the ribbon synthesized at 30 m/s has higher degree of short-range ordering. The formation of a glassy phase in these samples

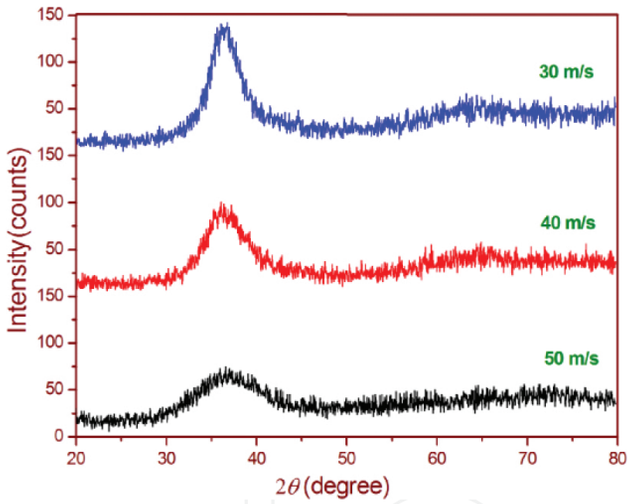

Figure 9. XRD patterns of as-synthesized ribbons of $Zr_{69.5}Ga_{7.5}Cu_{12}Ni_{11}$ metallic glass at wheel speed of 30, 40, and 50 m/s. (Reprinted with kind permission from reference [15], Copyright 2015, Elsevier.)

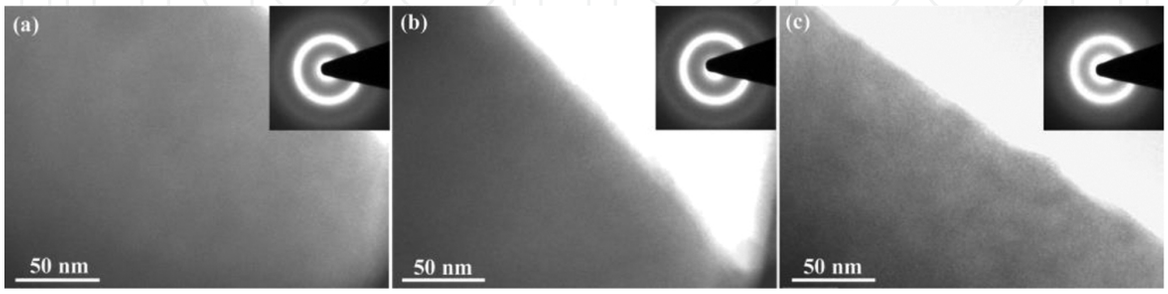

Figure 10. TEM micrographs with inset showing the selected area electron diffraction patterns of as-synthesized $Zr_{69.5}Ga_{7.5}Cu_{12}Ni_{11}$ alloys synthesized at wheel speeds (a) 50, (b) 40, and (c) 30 m/s. (Reprinted with kind permission from reference [15], Copyright 2015, Elsevier.)

was further investigated by TEM. **Figure 10** and the insets therein show the TEM micrographs and the corresponding selected area electron diffraction (SAED) patterns for $Zr_{69.5}Ga_{7.5}Cu_{12}Ni_{11}$ melt-spun alloys synthesized at 50, 40, and 30 m/s, respectively. We note that all TEM micrographs depict no discernible contrast and the corresponding SAED patterns displaying diffuse halos. This confirms to the XRD results presented above.

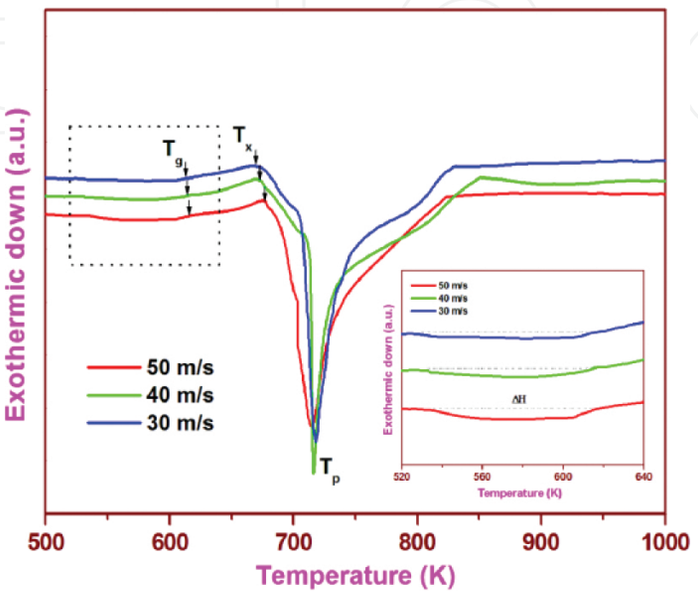

Figure 11. DSC curves of the as-synthesized $Zr_{69.5}Ga_{7.5}Cu_{12}Ni_{11}$ metallic glass samples synthesized under different cooling conditions. Inset highlights the enlarged section of the DSC curves below the glass transition temperature. (Reprinted with kind permission from reference [15], Copyright 2015, Elsevier.)

Figure 11 shows differential scanning calorimeter (DSC) scans taken at a heating rate of 20 K/min for the glassy alloys prepared under different cooling conditions. All DSC curves exhibited one clear endothermic heat event, characteristic of the glass transition to a supercooled liquid state, followed by only one single exothermic peak between about 670 and 820 K. It can be seen that the DSC curves of all the samples are very similar with glass transition temperature (T_g) in the range of 612–616 K and onset crystallization temperature (T_x) in the range of 670–676 K. This indicates the comparable thermal stability (ΔT_x) among the samples. **Table 2** summarizes the thermal stability data for all the investigated samples. The crystallization enthalpies can be obtained by integrating the area covered by the crystallization peak in the DSC curve and are found to be 61.1, 60.3, and 58.9 J/g for the ribbons synthesized at 50, 40, and 30 m/s, respectively. The crystallization enthalpy decreases with the decreasing cooling rate and thus confirming that the sample synthesized at 30 m/s contains a larger degree of short-range ordering or medium-range ordering. The degree of ordering can also be estimated by evaluating the crystallization fraction (V_f) of the sample from the DSC curves and is given by [72]:

$$V_f = \frac{\Delta H_{max} - \Delta H}{\Delta H_{max}} \tag{2}$$

where ΔH_{max} is the total enthalpy change when the fully amorphous alloy transforms into a completely crystallized one and ΔH is the crystallization enthalpy of the examining sample. Considering the sample synthesized at 50 m/s to be fully amorphous with zero crystallization fraction, the crystallization fraction for the samples synthesized at 40 and 30 m/s was found to be 1.3% and 3.6%, respectively, suggesting a negligible crystalline content in the samples. The small increase in the crystallization fraction results from the enhanced short-range ordering.

Cooling rate (m/s)	T_g (K)	T_x (K)	T_p (K)	ΔT_x (K)
30	612	670	718	58
40	614	673	716	59
50	616	676	714	60

T_g: glass transition temperature; T_x: onset crystallization temperature; ΔT_x: supercooled liquid region; T_p: exothermic peak.

Table 2. Thermal analysis of the melt-spun $Zr_{69.5}Ga_{7.5}Cu_{12}Ni_{11}$ ribbons synthesized at different cooling rate.(Reprinted with kind permission from reference [15], Copyright 2015, Elsevier.)

As evident from **Figure 11** and **Table 2**, there is a slight increase in the value of T_g, T_x, and ΔT_x with the increasing cooling rate. However, careful analysis reveals some differences around the glass transition regions, as more clearly seen in the inset of **Figure 11**. The inset of **Figure 11** is a local magnified region of the DSC curves below T_g, illustrating the heat release events due to structural relaxation. The structural relaxation enthalpy associated with the exothermic peak below T_g can be calculated by integrating the heat flow near the glass transition range (the area between the dotted lines and the curves shown in the inset of **Figure 11**). The relaxation enthalpy has been found to be 2.69, 3.98, and 5.84 J/g for the glassy ribbons synthesized at 30, 40, and 50 m/s, respectively, as provided in **Table 3**. A higher cooling rate has resulted in a larger relaxation enthalpy. Slipenyuk et al. [73] have shown that the exothermic heat release is directly related to the structural relaxation, i.e., the change of free volume in metallic glasses, and can be calculated by

$$(\Delta H)_{fv} = \beta \Delta_{vf} \tag{3}$$

where β is a constant, $(\Delta H)_{fv}$ is the change in enthalpy due to per unit free volume, and Δv_f is the change of free volume per atomic volume. Thus, the change in free volume of the glassy ribbons synthesized at different wheel speeds may be obtained by Eq. (3). Assuming that the free volume per atomic volume for the ribbon synthesized at 50 m/s to be ρ_o, the substitution of values of ΔH (cf. **Table 3** and the inset in **Figure 11**) into Eq. (3), the values of free volume per atomic volume for the ribbons synthesized at 40 and 30 m/s were found to be 0.68 ρ_o and 0.46 ρ_o, respectively. Such a computation suggests that the glassy ribbons synthesized at lower wheel speed have less free volume per atomic volume than the ribbons synthesized at higher wheel speed. The ribbons synthesized at 50 m/s are, therefore, believed to possess the highest

free volume. According to Turnbull and Cohen [74], the amount of free volume in a metallic glass is determined by the cooling rate. A slower cooling rate gives sufficient time to the atoms to attain their local ordered equilibrium positions, thereby, a more ordered atomic structure forms during cooling from the melt and thus, the obtained glassy sample has a smaller amount of free volume [69]. The amount of free volume in a metallic glass corresponds to the atomic packing density and one of the important parameters exerts a strong influence on the mechanical properties of the metallic glass.

Cooling rate (m/s)	Hardness (VHN) (GPa) (±0.10)	n	Log K	σ_0 (GPa) (100 g load) (±0.05)	$\alpha = A/A_s$	Crystallization enthalpy (ΔH) (J/g)	Structural relaxation enthalpy (J/g)
30	6.81	1.82	2.23	3.43	1.45	58.9	2.69
40	6.63	1.83	2.24	3.26	1.50	60.3	3.98
50	6.43	1.84	2.25	3.09	1.57	61.1	5.84

Table 3. Summary of hardness (VHN), Meyer's exponent (n), material constant (K), yield strength (σ_0), pileup parameter (α), crystallization enthalpy (ΔH) and structural relaxation heat of the Zr-based metallic glass samples with different cooling rate. (Reprinted with kind permission from reference [15], Copyright 2015, Elsevier.)

3.2. Mechanical properties

In this section, we present the results of cooling rate effect on the mechanical behavior of $Zr_{69.5}Ga_{7.5}Cu_{12}Ni_{11}$ MGs synthesized at different wheel speeds. The microhardness measurements were carried out by Vickers microhardness tester. The mean hardness reported here is

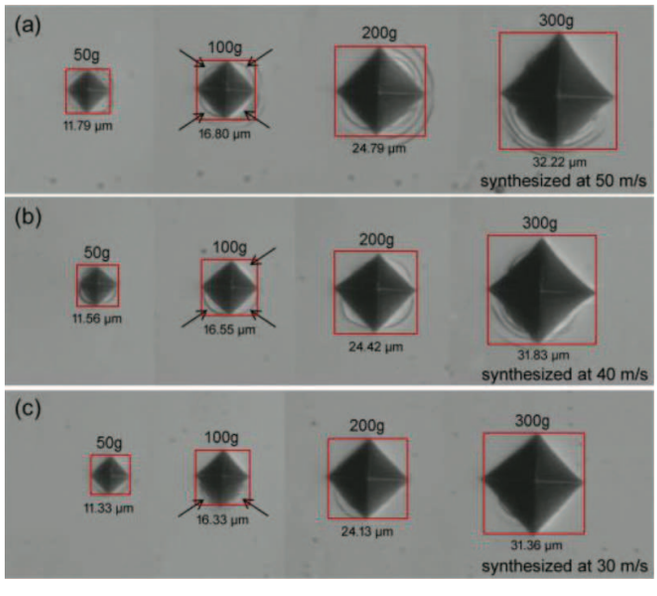

Figure 12. Indentation imprints at different loads for the as-synthesized ribbons of $Zr_{69.5}Ga_{7.5}Cu_{12}Ni_{11}$ metallic glass at wheel speed of (a) 50, (b) 40, and (c) 30 m/s showing the formation of shear bands around the indents. Four indentation impressions from various regions of the sample are superimposed. (Reprinted with kind permission from reference [15], Copyright 2015, Elsevier.)

http://dx.doi.org/10.5772/64221

the average of at least five points on each sample. **Figure 12** shows the representative optical micrographs of indents at different loads in $Zr_{69.5}Ga_{7.5}Cu_{12}Ni_{11}$ MGs synthesized at 50, 40, and 30 m/s, respectively. These micrographs reveal that the indents are crack free up to the load of 300 g for all the samples. The wavy patterns around the indent reveal the generation and formation of shear bands (marked by arrows in **Figure 12**). It can be clearly seen that the number of visible shear bands for the ribbons synthesized at 50 m/s is higher than those observed for the ribbons synthesized at 40 and 30 m/s. To further confirm this, we have calculated the pileup parameter. The characteristic spiral pattern around indents constitutes pileup and is related to the formation of shear bands. Pileups at which shear band reaches the surface are extensively observed around indents in amorphous alloys [19, 20]. The pileup parameter (α) can be calculated by employing the following relationship [75]:

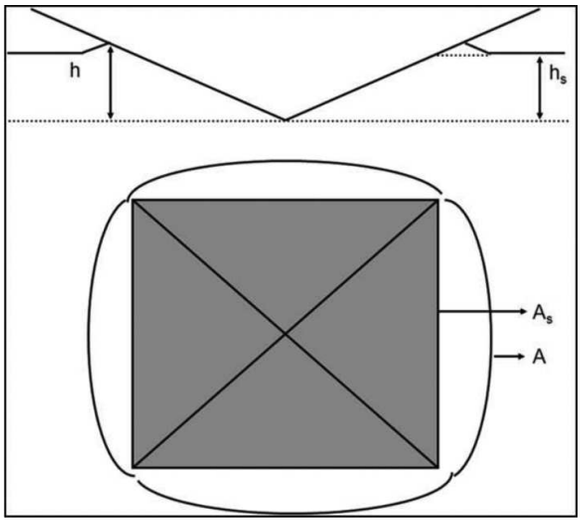

Figure 13. Schematic representation of various quantities used for calculation of pileup parameter (α) [75]; A_s and A are the area of impression before and after pileup, whereas h_s and h are the depth of impression before and after pileup.

$$\alpha = A/A_s \tag{4}$$

where $A_s = fh_s^2$ with f as a constant and is equal to 24.5 for Vickers pyramid indenter. The values of A_s and A are the area of impression before and after pileup, whereas h_s and h are the depth of impression before and after pileup. Various quantities utilized for the determination of α are displayed through a schematic diagram in **Figure 13**. The pileup area calculation was done by graphical methods. The values of α for the ribbons synthesized under different cooling conditions are reported in **Table 3**. The pileup parameter has been found to be maximum for the ribbons synthesized at 50 m/s. In contrast to this, the ribbons synthesized at 40 and 30 m/s are having relatively lower value of α indicates that few shear bands are generated during indentation. Among the three types of specimens, the ribbons synthesized at 50 m/s contain the large free volume and have the highest shear band density. The high free volume content not only favors the nucleation of shear bands but also helps to enhance the atomic mobility

that can alleviate the stress concentration and therefore prevent the metallic glass from cracking. Thus, it can be inferred that for the glassy alloy of fixed composition gives rise to the larger number of shear bands with higher cooling rate. Furthermore, higher free volume at enhanced cooling rates not only facilitates permanent flow of materials under compressive stresses but also contributes to enhancement in the fracture strength.

The hardness (H) was calculated in GPa units by employing the following relationship [76]:

$$\mathrm{H} = 1.854 \times 9.8 \times \frac{P}{d^2} \tag{5}$$

where P is the load (g) and d is the diagonal length in μm. **Figure 14(a)** shows hardness (VHN) versus load (g) characteristic curves for the ribbons synthesized at 30, 40, and 50 m/s, respectively. It can be seen from the load-dependent hardness curves (**Figure 14(a)**) that the hardness decreases with increase in the load due to indentation size effect (ISE) [77, 78]. **Table 3** compares the values of microhardness and other indentation parameters of the ribbons synthesized at different cooling rates. The hardness values of the ribbons synthesized at 30, 40, and 50 m/s at 100 g load are ~6.81, ~6.63, and ~6.43 GPa, respectively, clearly suggesting that faster the cooling rate during solidification, the lower the microhardness. The glass forming ability parameters and hardness values of $Zr_{69.5}Ga_{7.5}Cu_{12}Ni_{11}$ alloy synthesized at 50 m/s have been compared with some other known Zr-based alloys (cf. **Table 4**). Compared with the other typical MGs, $Zr_{69.5}Ga_{7.5}Cu_{12}Ni_{11}$ alloy has higher hardness but lower T_g and ΔT_x values. The hardness for $Zr_{69.5}Ga_{7.5}Cu_{12}Ni_{11}$ alloy is 6.43 GPa that is higher in comparison to the majority of the metallic glass alloy systems listed in **Table 4**.

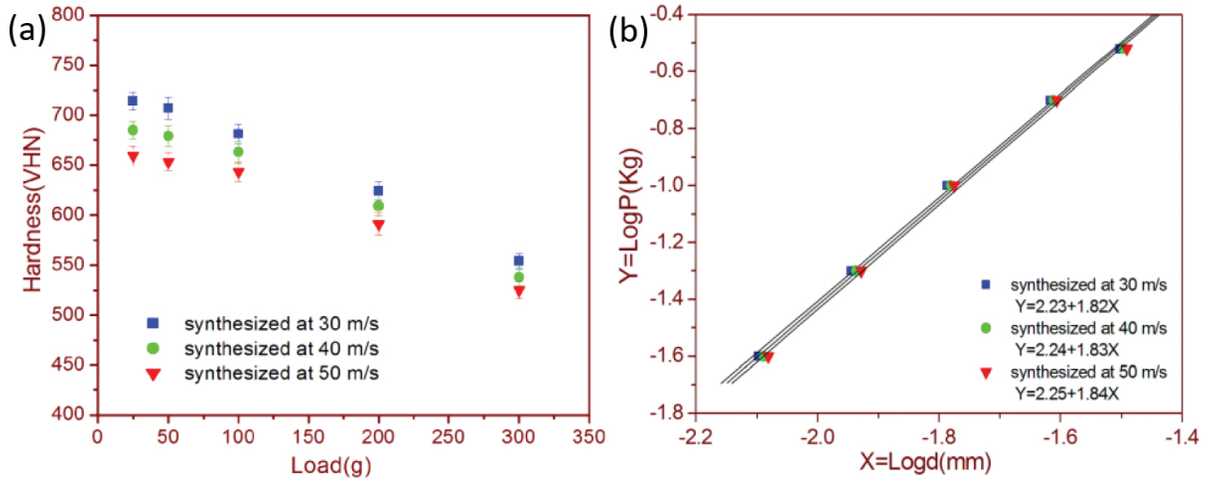

Figure 14. (a) Variation of hardness (VHN) with respect to load (g) for the as-synthesized ribbons of $Zr_{69.5}Ga_{7.5}Cu_{12}Ni_{11}$ metallic glass synthesized at different cooling rates. (b) Log P versus Log d plots for the as-synthesized ribbons of $Zr_{69.5}Ga_{7.5}Cu_{12}Ni_{11}$ metallic glass at wheel speed of 30, 40, and 50 m/s. (Reprinted with kind permission from reference [15], Copyright 2015, Elsevier.)

Alloys	T_g (K)	T_x (K)	ΔT_x (K)	Hardness (GPa)	Reference
$Zr_{41.2}Ti_{13.8}Cu_{12.5}Ni_{10}Be_{22.5}$	623	705	82	5.34	Raghavan etal. [50]
$Zr_{55}Pd_{10}Cu_{20}Ni_5Al_{10}$	696	775	79	5.28	Liu et al. [62]
$Zr_{55}Cu_{17.5}Al_{7.5}Ni_{10}Si_{10}$	700	748	48	7.20	Jang et al. [51]
$(Zr_{69.5}Al_{7.5}Cu_{12}Ni_{11})_{88}Ti_{12}$	628	686	58	6.00	Singh et al. [53]
$Zr_{51.9}Cu_{23.3}Ni_{10.5}Al_{4.3}$	705	801	96	5.50	Sun et al. [83]
$Zr_{51}Ti_5Ni_{10}Cu_{25}Al_9$	675	729	54	5.42	Sun et al. [83]
$Zr_{46}Cu_{37.6}Ag_{8.4}Al_8$	706	796	90	5.54	Sun et al. [83]
$Zr_{57}Cu_{27}Al_{11}Ni_5$	682	745	63	5.85	Jana et al. [67]
$Zr_{69.5}Al_{7.5}Cu_{12}Ni_{11}$	624	702	78	4.70	Singh et al. [20]
$Zr_{65}Al_{7.5}Cu_{17.5}Ni_{10}$	656	735	79	5.50	Jang et al. [51]
$Zr_{69.5}Ga_{7.5}Cu_{12}Ni_{11}$	616	676	60	6.43	Singh et al. [15]

Table 4. Comparison of T_g, T_x, ΔT_x and hardness values of $Zr_{69.5}Ga_{7.5}Cu_{12}Ni_{11}$ melt-spun alloy synthesized at 50 m/s with some other Zr-based metallic glasses.

The load independent hardness values permits us to compute the 0.2% offset yield strength (σ_0) by using the following relationship [79]:

$$\sigma_0 = (\mathrm{VHN}/3)0.1^{n-2} \tag{6}$$

where n = Meyer's exponent. This is determined by the slope log P (in Kg) versus log d (in mm) curve. The intercept of this curve K is the material constant related to the resistance of the metal to penetration. **Figure 14(b)** shows log P versus log d curves for the ribbons synthesized at different wheel speeds. The values of n and K are reported in **Table 3**. There is no significant variation observed in the values of n and K for the samples. The values of exponent are less than 2 as observed for intermetallics [80]. The yield strength lies in the range of ~3.09–3.43 GPa for the samples and is found to be maximum for the ribbon synthesized at 30 m/s. In the present case, both hardness and yield strength increase with decrease in the cooling rate and this may be attributed to the variation of free volume with the cooling rate. As the cooling rate decreases, the free volume decreases and thus causes densification of the metallic glass that results in an increased resistance to plastic deformation and therefore enhancement of hardness of the metallic glass upon structural relaxation [81–87].

4. Conclusion

In this chapter, the recent progress in the development of metallic glasses, quasicrystals and their nanocomposites are discussed. The $Zr_{69.5}Al_{7.5-x}Ga_xCu_{12}Ni_{11}$ system displayed metallic glass formation in the range of x = 0–7.5. In this process, we have come out with a new composition of glass without Al corresponding to x = 7.5. The nanohardness and reduced

elastic modulus values of the metallic glasses have been compared to their nanocomposites. The indentation characteristics of the glass composition with x = 7.5 have shown significant improvement in regard to hardness and elastic modulus. Based on transmission electron microscopic studies of the indented glassy specimen, the possibility of deformation-induced nanocrystallization has been ruled out.

In addition to, the cooling rate effect on the glass forming ability, crystallization and mechanical behavior of $Zr_{69.5}Ga_{7.5}Cu_{12}Ni_{11}$ metallic glass composition is presented. A slower cooling rate leads to higher degree of structural relaxation, less free volume content and therefore better short-range ordering. Such relatively ordered atomic configuration and less free volume content result in a higher hardness and yield strength for the samples synthesized at slower cooling rate than those synthesized at faster cooling rate. The ribbons synthesized at faster cooling rate contain the large free volume and have the highest shear band density. The glass forming ability parameters and hardness values of $Zr_{69.5}Ga_{7.5}Cu_{12}Ni_{11}$ alloy have shown significant improvement in comparison to some other known Zr-based alloys.

Acknowledgements

The authors are thankful to Dr. M.A. Shaz and Dr. T.P. Yadav for many stimulating discussions. One of the authors (Devinder Singh) gratefully acknowledges the financial support by Department of Science and Technology (DST), New Delhi, India in the form of INSPIRE Faculty Award [IFA12-PH-39]. Sections 2 and 3 of this chapter are reproduced with permission from References [15] and [19] (©2015, 2011 Elsevier).

Author details

Devinder Singh[1*], R.K. Mandal[2], R.S. Tiwari[3] and O.N. Srivastava[3]

*Address all correspondence to: devinderbhu@yahoo.com

1 Department of Physics, Panjab University, Chandigarh, India

2 Department of Metallurgical Engineering, Indian Institute of Technology (Banaras Hindu University), Varanasi, India

3 Department of Physics, Nano-Science Unit, Banaras Hindu University, Varanasi, India

References

[1] Telford M. The case for bulk metallic glasses. Mater Today. 2004;7:36.

[2] Ashby MF, Greer AL. Metallic glasses as structural materials. Scripta Mater. 2006;54:321.

[3] Kawamura Y, Ohno Y. Superplastic bonding of bulk metallic glasses using friction. Scripta Mater. 2001;45:279.

[4] Li M, Eckert J, Kecskes L, Lewandowski J. Mechanical properties of metallic glasses and applications. J Mater Res. 2007;22:255.

[5] Inoue A, Fan C, Saida J, Zhang T. High strength Zr-based bulk amorphous alloys containing nanocrystalline and nanoquasicrystalline particles. Sci TechnolAdv Mater. 2000;1:73.

[6] Shechtman D, Blech I, Gratias D, Cahn JW. Metallic phase with long-range orientational order and no translational symmetry. Phys Rev Lett. 1984;53:1951.

[7] Levine D, Steinhardt PJ. Quasicrystals. I. Definition and structure. Phys Rev B. 1986;34:596.

[8] Singh D, Yadav TP, Tiwari RS, Srivastava ON. Phase formation in rapidly quenched Cu-based alloys. J Mater Sci. 2009;44:3883.

[9] Zou XD, Fung KK, Kuo KH. Orientation relationship of decagonal quasicrystal and tenfold twins in rapidly cooled Al-Fe alloy. Phys Rev B. 1987;35:4526.

[10] Goldman AI, Kelton KF. Quasicrystals and crystalline approximants. Rev Mod Phys. 1993;65:213.

[11] Singh D, Yun Y, Wan W, Grushko B, Hovmöller S, Zou XD. A complex pseudo-decagonal quasicrystal approximant $Al_{37}(Co,Ni)_{15.5}$ solved by the rotation electron diffraction (RED) method. J Appl Crystallography. 2014;47:215.

[12] Singh D, Yun Y, Wan W, Grushko B, Hovmöller S, Zou XD. Structure determination of a pseudo-decagonal quasicrystal approximant by the strong-reflections approach and rotation electron diffraction. J Appl Crystallography. 2016;49:433-441. doi:10.1107/S1600576716000042.

[13] Misra DK, Sohn SW, Kim WT, Kim DH. Plastic deformation in nanostructured bulk glass composites during nanoindentation. Intermetallics. 2009;17:1.

[14] Singh D, Yadav TP, Mandal RK, Tiwari RS, Srivastava ON. Effect of Ga substitution on the crystallization behaviour and glass forming ability of Zr-Al-Cu-Ni alloy. Mater Sci Eng A. 2010;527:469.

[15] Singh D, Mandal RK, Tiwari RS, Srivastava ON. Effect of cooling rate on the crystallization and mechanical behaviour of Zr-Ga-Cu-Ni metallic glass composition. J Alloys & Compds. 2015;648:456.

[16] Koster U, Meinhardt J, Roos S, Liebertz H. Formation of quasicrystals in bulk glass forming Zr-Cu-Ni-Al alloys. Appl Phys Lett. 1996;69:179.

[17] Inoue A. Stabilization of metallic supercooled liquid and bulk amorphous alloys. Acta Mater. 2000;48:279.

[18] Wang WH, Dong C, Shek CH. Bulk metallic glasses. Mater Sci Eng R. 2004;44:45.

[19] Singh D, Mandal RK, Tiwari RS, Srivastava ON. Nanoindentation characteristics of $Zr_{69.5}Al_{7.5-x}Ga_xCu_{12}Ni_{11}$ glasses and their nanocomposites. J Alloys & Compds. 2011;509:8657.

[20] Singh D, Yadav TP, Mandal RK, Tiwari RS, Srivastava ON. Indentation characteristics of metallic glass and nanoquasicrystal-glass composite in Zr-Al(Ga)-Cu-Ni alloys. Intermetallics. 2010;18:2445.

[21] Singh D, Singh M, Yadav TP, Mandal RK, Tiwari RS, Srivastava ON. Nanoindentation studies of metallic glasses and nanoquasicrystal-glass composites in Zr-Al (Ga)-Cu-Ni alloys. Int J Nanosci. 2011;10:929.

[22] Kelton KF. Crystallization of liquids and glasses to quasicrystals. J Non-Cryst Solids. 2004;334 & 335:253.

[23] Mei JN, Li JS, Kon HC, Fu HZ, Zhou L. Effects of Nb on the formation of icosahedral quasicrystalline phase in Ti-rich Ti-Zr-Ni-Cu-Be glassy forming alloys. J Non-Cryst Solids. 2008;354:3332.

[24] Heinzig M, Jenks CJ, Hove MV, Fisher I, Canfield P, Thiel PA. Surface preparation and characterization of the icosahedral Al-Ga-Pd-Mn quasicrystal. J Alloys & Compds. 2002;338:248.

[25] Yadav TP, Singh D, Shahi RR, Shaz MA, Tiwari RS, Srivastava ON. Formation of quasicrystalline phase in $Al_{70-x}Ga_xPd_{17}Mn_{13}$ alloys. Phil Mag. 2011;91:2474.

[26] Yadav TP, Singh D, Shaz MA, Tiwari RS, Srivastava ON. Synthesis of quasicrystalline film of Al-Ga-Pd-Mn alloy. Thin Solid Films. 2013;534:265.

[27] Qiang JB, Zhang W, Xie G, Kimura H, Dong C, Inoue A. An in situ bulk $Zr_{58}Al_9Ni_9Cu_{14}Nb_{10}$ quasicrystal-glass composite with superior room temperature mechanical properties. Intermetallics. 2007;15:1197.

[28] Vaidyanathan R, Dao M, Ravichandran G, Suresh S. Study of mechanical deformation in bulk metallic glass through instrumented indentation. Acta Mater. 2001;49:3781.

[29] Kim JJ, Cho Y, Suresh SA, Argon S. Nanocrystallization during nanoindentation of a bulk amorphous metal alloy at room temperature. Science. 2002;295:654.

[30] Singh D, Tiwari RS, Srivastava ON, Mandal RK., R.C. Sobti, Anupama Kaushik, Bhupinder Singh and S.K. Tripathi Synthesis and mechanical properties of $Zr_{69.5}Ga_{7.5}Cu_{12}Ni_{11}$ metallic glass and nanoquasicrystal-glass composites. *Emerging Paradigms in Nanotechnology*. Pearson Education. Chennai, India. 2013;81. ISBN: 978-81-317-8991-9.

[31] Singh D, Mandal RK, Tiwari RS, Srivastava ON. Role of nano-quasicrystals in the formation of shear bands in Zr-based glassy alloys. *Nanotechnology: Novel Perspectives and Prospects*. McGraw-Hill, USA. 2015. ISBN: 978-93-392-2109-6.

[32] Singh D, Tiwari RS, Srivastava ON. *Metallic Glasses, Quasicrystals and Their Nanocomposites*. Lap Lambert Academic Publishing, Germany. 2014;111156:165. ISBN: 978-3-659-62088-1.

[33] Trexler MM, Thadhani NN. Mechanical properties of bulk metallic glasses. ProgMater Sci. 2010;55:759.

[34] Wang JG, Choi BW, Nieh TG, Liu CT. Crystallization and nanoindentation behavior of a bulk Zr-Al-Ti-Cu-Ni amorphous alloy. J Mater Res. 2000;15:798.

[35] Tariq NH, Hasan BA, Akhter JI, Ali F. Mechanical and tribological properties of Zr-Al Ni-Cu bulk metallic glasses. J Alloys & Compds. 2009;469:179.

[36] Ramamurty U, Nagendra N, Li Y. Variation in mechanical properties with crystallinity of a La-based bulk metallic glass. J Metastruct Mater. 2001;10:61.

[37] Qian L, Li M, Zhou Z, Yang H, Shi X. Comparison of nano-indentation hardness to microhardness. Surf Coat Technol. 2005;195:264.

[38] Drozdz D, Kulik T, Fecht HJ. Nanoindentation studies of Zr-based bulk metallic glasses. J Alloys Compds. 2007;441:62.

[39] Azad S, Mandal A, Mandal RK. On the parameters of glass formation in metallic systems. Mater Sci Eng. A 2007;458:348.

[40] Anthony Fischer-Cripps C. *Nano-Indentation, Mechanical Engineering Series*. Frederick F. Ling (Series ed.), Springer-Verlag, New York. 2004.

[41] Jang JSC, Jian SR, Chang CF, Chang LJ, Huang YC, Li TH, Huang JC, Liu CT. Thermal and mechanical properties of the $Zr_{53}Cu_{30}Ni_9Al_8$ based bulk metallic glass microalloyed with silicon. J Alloys & Compds. 2009;478:215.

[42] Jiang WH, Pinkerton FE, Atzmon M. Mechanical behavior of shear bands and the effect of their relaxation in a rolled amorphous Al-based alloy. Acta Mater. 2005;53:3469.

[43] Schuh CA, Hufnagel TC, Ramamurty U. Mechanical behavior of amorphous alloys. Acta Mater. 2007;55:4067.

[44] Dubach A, Dalla Torre FH, Loffler JF. Constitutive model for inhomogeneous flow in bulk metallic glasses. Acta Mater. 2009;57:881.

[45] Uhhenhaut DI, Dalla Torre FH, Castellero A, Gomez CAP, Djowrelon N, Krauss G, Schmitt B, Patterson B, Loffler JF. Structural analysis of rapidly solidified Mg-Cu-Y glasses during room-temperature embrittlement. Phil Mag. 2009;89:233.

[46] Xie S, George EP. Hardness and shear band evolution in bulk metallic glasses after plastic deformation and annealing. Acta Mater. 2008;56:5202.

[47] Yoo BG, Park KW, Lee JC, Ramamurty U, Jang JI. Role of free volume in strain softening of as-cast and annealed bulk metallic glass. J Mater Res. 2009;24:1405.

[48] Mandal RK, Tiwari RS, Singh D, Singh D. Influence of Ga substitution on the mechanical behavior of $Zr_{69.5}Al_{7.5-x}Ga_xCu_{12}Ni_{11}$ and $Ce_{75}Al_{25-x}Ga_x$metallic glass compositions. MRS Proceeding. 2015;1757. doi:10.1557/opl.2015.45.

[49] Singh D, Shahi RR, Yadav TP, Mandal RK, Tiwari RS, Srivastava ON. Hydrogenation of $(Zr_{69.5}Al_{7.5}Cu_{12}Ni_{11})_{100-x}Ti_x$ quasicrystalline alloys and its effect on their structural and microhardness behaviour. J Non-Cryst Solids. 2013;380:11.

[50] Raghavan R, Murali P, Ramamurty U. Ductile to brittle transition in the $Zr_{41.2}Ti_{13.75}Cu_{12.5}Ni_{10}Be_{22.5}$ bulk metallic glass. Intermetallics. 2006;14:1051.

[51] Jang JSC, Chen YW, Chang LJ, Cheng HZ, Huang CC, Tsau CY. Crystallization and fracture behavior of the $Zr_{65-x}Al_{7.5}Cu_{17.5}Ni_{10}Si_x$ bulk amorphous alloys. Mater Chem Phys. 2005;89:122.

[52] Huang YJ, Shen J, Sun JF. Bulk metallic glass: smaller is softer. Appl Phys Lett. 2007;90:081919.

[53] Singh D, Yadav TP, Mandal RK, Tiwari RS, Srivastava ON. Effect of Ti addition on the quasicrystalline phase formation and indentation characteristics of $Zr_{69.5}Al_{7.5}Cu_{12}Ni_{11}$ alloy. Phil Mag. 2011;91:2837.

[54] Dubach A, Prasad KE, Raghavan R, Löffler JF, Michler J, Ramamurty U. Free-volume dependent pressure sensitivity of Zr-based bulk metallic glass. J Mater Res. 2009;24:2697.

[55] Ye JC, Lu J, Liu CT, Wang Q, Yang Y. Atomistic free volume zones and inelastic deformation of metallic glasses. Nat Mater. 2010;9:619.

[56] Xu Y, Shi B, Ma Z, Li J. Evolution of shear bands, free volume and structure in room temperature rolled $Pd_{40}Ni_{40}P_{20}$ bulk metallic glass. Mater Sci & Eng A. 2015;623:145.

[57] Zhu ZD, Ma E, Xu J. Elevating the fracture toughness of $Cu_{49}Hf_{42}Al_9$ bulk metallic glass: effects of cooling rate and frozen-in excess volume. Intermetallics. 2014;46:164.

[58] Evenson Z, Koschire T, Wei S, Gross O, Bednarcik J, Gallino I, Kruzic JJ, Rätzke K, Faupel F, Busch R. The effect of low-temperature structural relaxation on free volume and chemical short-range ordering in a $Al_{49}Cu_{26.9}Si_{16.3}Ag_{5.5}Pd_{2.3}$ bulk metallic glass. Scripta Mater. 2015;103:14.

[59] Tan J, Wang G, Liu ZY, Bednarclk J, Gao YL, Zhai QJ, Mattern N, Eckert J. Correlation between atomic structure evolution and strength in a bulk metallic glass at cryogenic temperature. Sci Reports. 2014;4. doi:10.1038/srep03897.

[60] Cheng YQ, Cao AJ, Sheng HW, Ma E. Local order influences initiation of plastic flow in metallic glass effects of alloy composition and sample cooling history. Acta Mater. 2008;56:5263.

[61] Chen M. A brief overview of bulk metallic glasses. NPG Asia Mater. 2011;3:82.

[62] Liu ZY, Yang Y, Guo S, Liu XJ, Lu J, Liu YH, Liu CT. Cooling rate effect on Young's modulus and hardness of a Zr-based metallic glass. J Alloys & Compds. 2011;509:3269.

[63] Hu Y, Yan HH, Lin T, Li JF, Zhou YH. Effect of cooling rate on the bending plasticity of $Zr_{55}Al_{10}Ni_5Cu_{30}$ bulk metallic glass. J Alloys & Compds. 2012;527:36.

[64] Liu Y, Bei H, Liu CT, George EP. Cooling-rate induced softening in a $Zr_{50}Cu_{50}$ bulk metallic glass. Appl Phys Lett. 2007;90:071909.

[65] Shen J, Huang YJ, Sun JF. Plasticity of a TiCu-based bulk metallic glass: effect of cooling rate. J Mater Res. 2007;22:3067.

[66] Misra DK, Sohn SW, Kim WT, Kim DH. Rate-dependent serrated flow and plastic deformation in $Ti_{45}Zr_{16}Be_{20}Cu_{10}Ni_9$ bulk amorphous alloy during nanoindentation. Sci Technol Adv Mater. 2008;9:045004.

[67] Jana S, Bhowmick R, Kawamura Y, Chattopadhyay K, Ramamurty U. Deformation morphology underneath the Vickers indent in a Zr-based bulk metallic glass. Intermetallics. 2004;12:1097.

[68] Chen LY, Setyawan AD, Kato H, Inoue A, Zhang GQ, Saida J, Wang XD, Cao QP, Jiang JZ. Free-volume-induced enhancement of plasticity in a monolithic bulk metallic glass at room temperature. Scripta Mater. 2008;59:75.

[69] Jiang WH, Liu FX, Wang YD, Zhang HF, Choo H, Liaw PK. Comparison of mechanical behavior between bulk and ribbon Cu-based metallic glasses. Mater Sci Eng A. 2006;430:350.

[70] Huang Y, Chiu YL, Shen J, Chen JJ, Sun J. Cooling rate effect of nanomechanical response for a Ti-based bulk metallic glass. J Non-Cryst Solids. 2010;356:966.

[71] Huang Y, Fan H, Wang D, Sun Y, Liu F, Shen J, Sun J, Mi J. The effect of cooling rate on the wear performance of a ZrCuAlAg bulk metallic glass. Materials & Design. 2014;58:284.

[72] Zhang LC, Jiang F, Zhang DH, He L, Sun J, Fan JT, Zhang ZF. In-situ precipitated nanocrystals beneficial to enhanced plasticity of Cu-Zr based bulk metallic glasses. Adv Eng Mater. 2008;10:943.

[73] Slipenyuk A, Eckert J. Correlationbetween enthalpy change and free volume reduction during structural relaxation of $Zr_{55}Cu_{30}Al_{10}Ni_5$ metallic glass. Scripta Mater. 2004;50:39.

[74] Turnbull D, Cohen MH. On the free-volume model of the liquid-glass transition. J Chem Phys. 1970;52:3038.

[75] Casals O, Alcala J. The duality in mechanical property extractions from Vickers and Berkovich instrumented indentation experiments. Acta Mater. 2005;53:3545.

[76] Mukhopadhyay NK, Weatherly GC, Embury JD. An analysis of microhardness of single-quasicrystals in the Al-Cu-Co-Si system. Mater Sci Eng A. 2001;315:202.

[77] Mukhopadhyay NK, Paufler P. Micro and nanoindentation techniques for mechanical characterization of materials. Int Mater Rev. 2006;51:209.

[78] Singh D, Singh D, Yadav TP, Mandal RK, Tiwari RS, Srivastava ON. Synthesis and indentation behaviour of amorphous and nanocrystalline phases in rapidly quenched Cu-Ga-Mg-Ti and Cu-Al-Mg-Ti alloys. Metallogr Microstruct Anal. 2013;2:321.

[79] Cahoon JR, Broughton WH, Kutzak AR. The determination of yield strength from hardness measurements. Metall Trans. 1971;2:1979.

[80] Mukhopadhyay NK, Bhatt J, Pramanik AK, Murty BS, Paufler P. Synthesis of nanocrystalline/nanoquasicrystalline $Mg_{32}(AlZn)_{49}$ by melt spinningand mechanical alloying. J Mater Sci. 2004;39:5155.

[81] Uhlenhaut DI, Dalla Torre FH, Castellero A, Gomez CAP, Djourelov N, Krauss G, Schmitt B, Patterson B, Löffler JF. Structural analysis of rapidly solidified Mg-Cu-Y glasses during room-temperature embrittlement. Phil Mag. 2009;89:233.

[82] Singh D, Singh D, Mandal RK, Srivastava ON, Tiwari RS. Glass forming ability, thermal stability and indentation characteristics in $Ce_{75}Al_{25-x}Ga_x$ metallic glasses. J. Alloys & Compds. 2014;590:15.

[83] Sun Y, Huang Y, Fan H, Liu F, Shen J, Sun J, Chen JJJ. Comparison of mechanical behaviours of several bulk metallic glasses for biomedical application. J Non-Cryst Solids. 2014;406:144.

[84] Singh D, Mandal RK, Srivastava ON, Tiwari RS. Glass forming ability, thermal stability and indentation characteristics of $Ce_{60}Cu_{25}Al_{15-x}Ga_x$ ($0 \le x \le 4$) metallic glasses. J Non-Cryst Solids. 2015;427:98.

[85] Singh D, Basu S, Mandal RK, Srivastava ON, Tiwari RS. Formation of nano-amorphous domains in $Ce_{75}Al_{25-x}Ga_x$ alloys with delocalization of cerium 4f electrons. Intermetallics. 2015;67:87.

[86] Singh D, Singh D, Srivastava ON, Tiwari RS. Microstructural effect on the low temperature transport properties of Ce-Al (Ga) metallic glasses. Scripta Mater. 2016;118:24.

[87] Yadav TP, Singh D, Tiwari RS, Srivastava ON. Enhanced microhardness of mechanically activated carbon-quasicrystal composite. Mater Lett. 2012;80:5.